

J. F. Gülich

Abstract The power losses created by the shrouds of closed turbomachine impellers depends on Reynolds-number, surface roughness, rate and direction of leakage flow through the impeller side room and on the pre-swirl with which said leakage enters the side room. These parameters determine also fluid rotation between impeller and casing and axial thrust. While all of these effects have been treated in the literature, a generic procedure has been lacking, which would allow to predict, in a consistent and logical way, the impact of all of these boundary conditions on disk friction and fluid rotation. To fill this gap a method is presented and validated with test data. The formulae developed cover laminar, turbulent, smooth and rough flow regimes and ensure a smooth transition between these domains.

Radreibungsverluste geschlossener Laufräder von Turbomaschinen

Zusammenfassung Der Leistungsverlust rotierender Radseitenwände in Turbomaschinen hängt ab von Reynolds-Zahl, Oberflächenrauheit, Betrag und Richtung etwaiger Leckagen und dem Vordrall besagter Leckage am Eintritt in den Radseitenraum. Diese Größen bestimmen auch die Rotation des Fluids zwischen Gehäuse und Laufrad sowie den Axialschub. Obwohl alle diese Effekte in der Literatur behandelt wurden, fehlte bisher ein allgemeingültiges Verfahren, mit dem die Auswirkung obiger Parameter auf die Radreibungsverluste und Fluidrotation vorausberechnet werden kann. Ein solches Verfahren wird im folgenden vorgestellt und anhand von Versuchsdaten überprüft. Die entwickelten Formeln sind gültig für laminare und turbulente Strömung, für glatte und raue Oberflächen sowie für die Übergangsbereiche zwischen diesen Strömungsformen.

List of symbols

c_f friction coefficient of a flat plate, Eq. (T2.3)
 c_u circumferential absolute velocity
 f_L factor accounting for net through flow
 $f_L \equiv k_{RR}(Q_{sp})/k_{RR}(Q_{sp} = 0)$

f_R factor accounting for effect of roughness on disk friction
 k rotation coefficient (side room flow) $k = \beta/\omega$, Eq. (T2.1)
 k_E rotation at inlet to gap A or to side room if $x_{ov} = 0$, Fig. 1
 k_z rotation at the outlet of gap A
 k_o fluid rotation in side room without through flow, Eq. (T1.3)
 k_{RR} disk friction factor, Table 1
 M torque
 n_q specific speed $n_q = nQ^{0.5}/H^{0.75}$ (rpm, m³/s, m)
 P_{RR} disk friction power loss of impeller side disks Eq. (T1.2)
 Q_{sp} leakage flow rate through impeller neck ring Fig. 1
 Q_{s3} leakage flow rate through inter-stage seal Fig. 1
 Re Reynolds-number, Eq. (T1.1)
 r_2 impeller outer radius
 r_w outer side room radius, Table 1
 s_{ax} width of axial gap between impeller and casing, Table 1
 t_{ax} cylindrical portion of impeller side room with r_w , Table 1
 x_{ov} overlap between impeller side disks and casing, Fig. 1
 z axial coordinate

Greek variables

β angular velocity of fluid rotation in side room
 ε equivalent sand roughness
 ε_{CLA} average depth of roughness (CLA, AA)
 ε_{max} maximum depth of roughness
 ε_τ eddy viscosity
 η_h hydraulic efficiency: $\eta_h = H/H_{th}$
 ν kinematic viscosity
 ρ density
 φ_{sp} leakage flow coefficient, Eq. (T2.1)
 ω angular rotor velocity

Subscripts, superscripts, abbreviations

* referred to impeller outer radius or diameter; e.g. $r_{sp}^* = r_{sp}/r_2$ or $d_{sp}^* = d_{sp}/d_2$
 2 impeller outlet (flow through pump)
 case casing wall (in impeller side room)
 imp impeller side disk (hub or shroud)
 in inlet to side room
 sp gap, leakage flow

Received: 15 March 2003

J. F. Gülich
 Ecole Polytechnique, LMH, Avenue de Cour 33Bis,
 CH 1007 Lausanne, Switzerland
 e-mail: johann.guelich@epfl.ch

1 Introduction

The side plates of shrouded impellers of pumps, compressors or hydraulic turbines generate drag losses when rotating in a fluid. These “disk friction losses” have an important impact on the efficiency of centrifugal machines with low or moderate specific speed: at $n_q = 10$ the disk friction power losses P_{RR} amount typically to about 50% of the useful power, while at $n_q = 30$ this fraction is about 5%. Wall shear stresses on the rotating body entrain the liquid, setting the fluid in the side room into rotation, and centrifugal forces in the boundary layer of the rotating disk induce a flow between said disk and the adjacent casing wall (“impeller side room flow”). The fluid rotation determines the pressure distribution on the impeller front and rear shroud and influences thus the axial forces on the impeller.

Disk friction losses and the flow in the impeller side rooms have therefore found considerable attention in the literature; comprehensive lists of relevant publications are given in [1, 2]. A complete review of these publications would take the form of a book rather than a journal contribution; therefore only a fraction of the work can be quoted subsequently. Earlier experiments on disk friction losses were done with a simple disk rotating in a cylindrical casing, e.g. [3–6], and empirical correlations of disk friction factors k_{RR} as function of Reynolds-number Re and equivalent sand roughness were derived from such tests. Later it was recognised that any leakage flow through the side room can influence significantly the pressure distribution on the impeller shrouds and the disk friction itself [7–13]. These investigations demonstrated that disk friction and the flow in the impeller side room depend on the following parameters: (1) Reynolds-number Re ; (2) surface roughness ε ; (3) direction and rate of (leakage) flow Q_{sp} through the side room; (4) the circumferential absolute velocity $c_{u,in}$ with which the leakage enters the side room; and (5) geometry. While some aspects of these parameters have been treated in numerous publications, a generic procedure was lacking which allows to account, in a rational way, for all of these effects when calculating disk friction losses. It is the purpose of the present paper to provide this type of procedure and validate it with test data. The discussion is limited to shrouds without pump-out vanes, which can be calculated by procedures given in [12].

2 Impeller side-room flow parameters

Figure 1 shows an impeller of a multi-stage pump (or compressor) where impeller neck ring leakage Q_{sp} flows radially *inwards* on the front shroud while the inter-stage seal allows a leakage Q_{s3} on the hub flowing radially *outwards*. With zero leakage centrifugal forces in the boundary layer on the rotating disk induce a circulation in the side-room, since the fluid pumped out by the disk must return on the casing wall to conserve continuity. In turbulent flow with separated boundary layers there is a core flow with essentially zero velocity gradient (which implies also zero shear stress) as sketched in the velocity profiles in Fig. 1. This core is usually described by the ratio

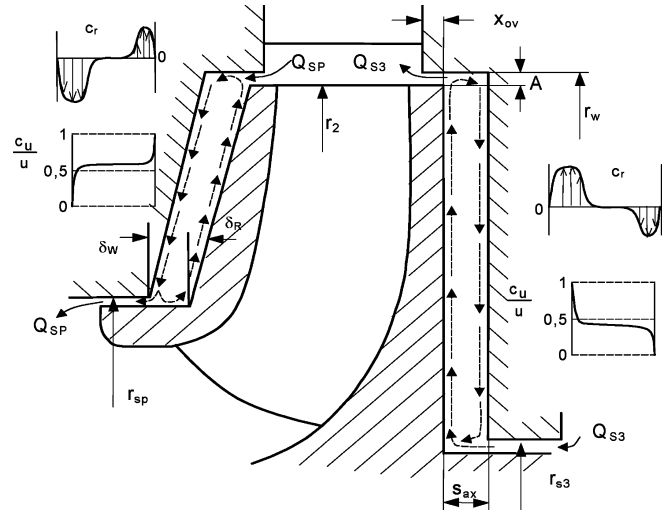


Fig. 1. Impeller side room flow ($x_{ov} > 0$, $t_{ax} = s_{ax}$)

of fluid velocity c_u to impeller circumferential velocity $u = \omega r$ expressed by the rotation factor $k = f(r)$.

$$k = \frac{c_u}{u} = \frac{c_u}{\omega r} = \frac{\beta}{\omega} \quad (1)$$

With zero leakage the rotation factor becomes independent from the radius, $k = k_o$, and depends only on the geometry of the side-room; k_o can be calculated from empirical formulae, e.g. (T1.3) which has been adapted from [7].

Any leakage flow Q_{sp} is superposed on the circulation flow pattern discussed above. The leakage flow carries a moment of momentum into the side-room which is proportional to the leakage flow rate and the circumferential velocity at the location where the leakage enters the side-room; it is thus given by

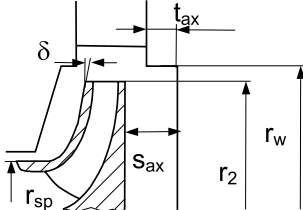
$$M_{sp} = \rho Q_{sp} r_{in} c_{u,in} = \rho Q_{sp} r_{in}^2 k_E \omega \quad (2)$$

$k_E = c_{u,in}/u_{in}$ is the rotation factor at the side-room inlet. If the leakage flows radially inwards, Q_{sp} enters the side room at the impeller outer radius r_2 with $k_E = c_{2u}/u_2$. In case of an inter-stage seal the leakage Q_{s3} enters the side room at r_{s3} and k_E must be calculated with the circumferential velocity component at the outlet of the inter-stage seal. $k_E = c_{u,in}/u_{in} = 0.25$ to 0.5 may be expected (depending on the length of the seal) or it may be calculated from Sec. 4.2 below.

Without friction, conservation of momentum would imply $c_u = c_{u,in} r_{in}/r$. When the leakage flows radially inwards, two cases may be considered: (1) If $k_E > k_o$ the leakage flow tends to accelerate the core flow and thus to decrease disk friction losses. (2) If $k_E < k_o$ the leakage flow tends to slow down the core flow and disk friction increases, since the impeller side disk has to accelerate the rotation of the leakage flow, hence takes more power. The disk friction factor is thus a complex function as described by (3)

$$k_{RR} = f\{Re, k_o(r_w^*, t_{ax}^*, c_f, imp, c_f, case), \varepsilon_{imp}, \varphi_{sp}, k_E, s_{ax}^*\} \quad (3)$$

Table 1. Friction losses of rotating disks. Various friction factor definitions are used in the references; in the present contribution all correlations from references were converted to the definition implied by Eq. (T1.2)

			Eq.
Reynolds-number	$Re = \frac{\omega r_2^2}{\nu}$	$s_{ax}^* = \frac{s_{ax}}{r_2}$	1.1
Friction power <i>per side</i> of a rotating disk, use for $\delta < 45^\circ$ only	$P_{RR} = \frac{k_{RR}}{\cos \delta} \rho \omega^3 r_2^5 \left\{ 1 - \left(\frac{r_1}{r_2} \right)^5 \right\}$		1.2
Rotation of fluid with zero leakage ($Q_{sp} = 0$). For open side rooms: $r_w = r_2$; $t_{ax} = 0$	$k_o = \frac{1}{1 + \left(\frac{r_w}{r_2} \right)^2 \sqrt{\left(\frac{r_w}{r_2} + 5 \frac{t_{ax}}{r_2} \right) \frac{C_{f, case}}{C_{f, imp}}}}$		1.3
Disk friction factors for different flow regimes [4]	$k_{RR} = \frac{\pi}{2Re s_{ax}^*}$	$Re_{lam} \leq \frac{8.7}{(s_{ax}^*)^{1.87}}$	Laminar, merged boundary layers 1.4
	$k_{RR} = \frac{0,925}{Re^{0,5}} (s_{ax}^*)^{0,1}$	$Re_{lam} < Re < 2 \times 10^5$	Laminar, separated boundary layers 1.5
	$k_{RR} = \frac{0,02}{(s_{ax}^*)^{1/6} Re^{0,25}}$	$10^5 < Re < 10^6$	Turbulent, merged boundary layers 1.6
	$k_{RR} = \frac{0,0255}{Re^{0,2}} (s_{ax}^*)^{0,1}$	$Re > 2 \times 10^5$	Turbulent, separated boundary layers 1.7
Disk friction factors covering all flow regimes [3, 12]	$k_{RR} = \frac{\pi}{2Re s_{ax}^*} + \frac{0,02}{Re^{0,2}} \cdot \frac{1 + s_{ax}^*}{1 + 0.5s_{ax}^*} f_{R, imp} f_L$		• valid for $Re > 10$ 1.8
Accounting for different factors which have an influence on k_o	$k_{RR} = \frac{\pi}{2Re s_{ax}^*} + \frac{0,0625}{Re^{0,2}} \cdot (1 - k_o)^{1,75} f_{R, imp} f_L$		• k_{RR} is <i>per side</i> of the disk 1.9
Roughness effect on disk friction	$f_{R, imp} \equiv \frac{k_{RR}(\varepsilon)}{k_{RR}(\varepsilon = 0)} = \left\{ \frac{\log \frac{12,5}{Re}}{\log \left(0,2 \frac{\varepsilon}{r_2} + \frac{12,5}{Re} \right)} \right\}^{2,15}$		Calculated with equivalent sand roughness ε of impeller side disks 1.10
Influence of leakage on disk friction, valid for: $r_{sp}/r_2 > 0.3$ and $k_E \approx 0.5$	$f_L \equiv \frac{k_{RR}(Q_{sp})}{k_{RR}(Q_{sp} = 0)} = \exp \left\{ -350 \varphi_{sp} \left(\left[\frac{r_2}{r_{sp}} \right]^a - 1 \right) \right\}$		Direction of leakage flow: radially inwards: φ_{sp} positive; $a = 1.0$; radially outwards: φ_{sp} negative; $a = 0.75$ 1.11
Influence of leakage on rotation factor k valid for: $r_{sp}/r_2 > 0.3$ and $k_E \approx 0.5$	$\frac{k_{cp}}{k_o} = \exp \left\{ 300 \varphi_{sp} \left(\left[\frac{r_2}{r_{sp}} \right]^b - 1 \right) \right\}$		Direction of leakage flow: radially inwards: φ_{sp} positive; $b = 1.0$; radially outwards: φ_{sp} negative; $b = 0.65$ 1.12
Power absorbed by a rotating cylinder with radius R	$P_{RZ} = k_{RZ} \rho \omega^3 R^4 L$		L = axial length of cylinder 1.13
	$k_{RZ} = \frac{2\pi R}{Re s} + \frac{0,075}{Re^{0,2}} \cdot \frac{1 + \frac{s}{R}}{1 + \frac{s}{2R}} \cdot f_R$		s = radial clearance between cylinder and stator part 1.14

3 Disk rotating in a cylindrical casing without through flow

The power absorbed by a smooth disk rotating in a cylindrical casing without net through flow has been measured extensively, e.g. [3–6]. Although geometric and flow parameters in actual pumps can be quite different from this simple model, it remains the basis for estimating disk friction losses, when properly extended by methods to account for net flow through the side room (if any).

3.1 Smooth disks

The disk friction losses can be calculated from Table 1, where Eq. (T1.1) defines the Reynolds-number and Eq. (T1.2) the power loss P_{RR} *per side* of the disk. k_{RR} is the experimental friction factor. Widely used correlations for k_{RR} are those measured by Dailey and Neece [4] as given in Eqs. (T1.4–1.7) which use four equations to cover the different flow regimes from laminar flow with merged boundary layers to turbulent flow with separated boundary

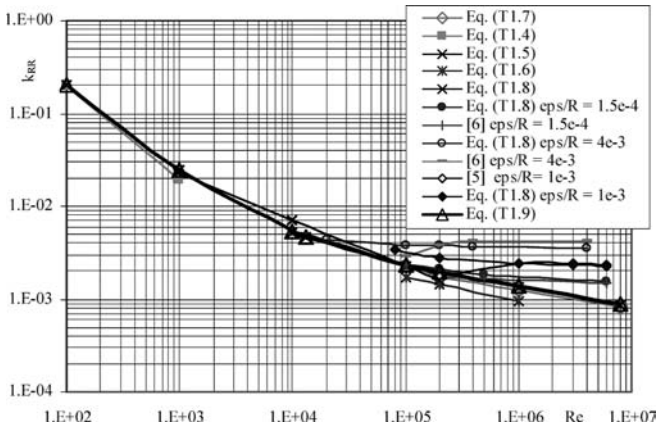


Fig. 2. Disk friction factor correlations for smooth and rough surfaces; $f_L = 1.0$ no leakage

layers. Based on measurements by Pantell [3], Linneken [14] derived a single formula to cover all flow regimes. Linneken's formula has been extended by Gülich [12] by the factors f_R and f_L to account for the effects of roughness and leakage, yielding Eq. (T1.8). In Eq. (T1.2) $\cos \delta$ has been introduced to account for inclined impeller shrouds; more complex impeller contours may be calculated in several sections.

Figure 2 demonstrates that Eq. (T1.8) agrees well with Eqs. (T1.4–1.7). Figure 2 was calculated with an axial clearance ratio $s_{ax}/R = 0.08$ (except for the roughness test data discussed below). In the laminar flow range s_{ax}/R has a strong influence on disk friction while in turbulent flow the impact is very small as demonstrated by many published test data. In the turbulent region Eq. (T1.8) depends less strongly on s_{ax}/R than Eq. (T1.7). Equation (T1.8) may be extrapolated to s_{ax}/R close to zero and infinite, while Eq. (T1.7) would give unreasonable friction factors for extreme values of s_{ax}/R . $s_{ax}/R = \text{infinite}$ corresponds to a free disk for which Eq. (T1.8) yields friction factors about 10% higher than the correlation $k_{RR} = 0.0365/Re^{0.2}$ given in [15].

During the present study a new equation has been developed. It combines the laminar term of Eq. (T1.8) with a correlation for turbulent flow given by Möhring [8], but the constant has been adapted to better fit the test data from [3 and 4] and the factors f_R and f_L have been introduced too. The resulting correlation is given as Eq. (T1.9) and plotted also in Fig. 2 which demonstrates that Eqs (T1.8) and (T1.9) are equivalent. Equation (T1.9) has however the important advantage, that all factors which have an impact on k_o are taken into account.

3.2

Impact of roughness on disk friction and fluid rotation

Tests were carried out by Neece [5] and Fukuda [6] with disks of varying roughness in a cylindrical casing without through flow. Disk and casing had the same roughness, in which case the core flow – or rotation factor k_o – is not affected by the roughness. While [5 and 6] gave correlations for fully rough surfaces the transition between rough and smooth surfaces, where pumps often operate, was not described. The use of *uniform* sand roughness in the

tests further lead to a minimum in $k_{RR} = f(Re)$ for any given roughness, which is expected to be absent with *non-uniform* technical roughness.

In order to get a generic expression covering smooth, transition and rough flows, a roughness factor f_R , Eq. (T1.10) has been derived from flat plate friction coefficients [12, 16]: at a given Reynolds-number f_R is the ratio of the friction on a rough plate to that on a smooth plate $f_R = c_f(\epsilon > 0)/c_f(\epsilon = 0)$. f_R smoothly approaches 1.0 when the Reynolds-number is reduced for a given roughness; the transition rough to smooth is thus well covered. As demonstrated by Fig. 2 Eqs. (T1.8 and 1.10) agree reasonably well with the test data of [5 and 6].

In order to calculate the roughness factor f_R from Eq. (T1.10) the equivalent sand roughness ϵ must be used. The problem of defining an appropriate roughness is not fully solved, which accounts for the differences between prediction and test in Fig. 2 (the roughness topic has been discussed in detail in [16]). When the impeller side disks and/or casing walls are machined and roughness grooves are thus in tangential direction such grooves have little effect on disk friction: Geis [17] found virtually no increase in disk friction when increasing the roughness from a polished to a machined surface with $\epsilon_{max} = 120 \mu\text{m}$. For cast surfaces the equivalent sand roughness can be estimated from $\epsilon = \epsilon_{max}/c_{eq}$ (with the roughness equivalence factor $c_{eq} = 2.6$ and $\epsilon_{max} = \text{maximum roughness depth}$), [16].

When impeller side disks and casing walls have different roughness ($\epsilon_{imp} \neq \epsilon_{case}$) the core flow in the impeller side room is affected: with $\epsilon_{imp} > \epsilon_{case}$ the core flow is accelerated (k_o increases) and when $\epsilon_{imp} < \epsilon_{case}$ the core flow is slowed down (k_o decreases). These effects of different impeller and casing roughness are well described by

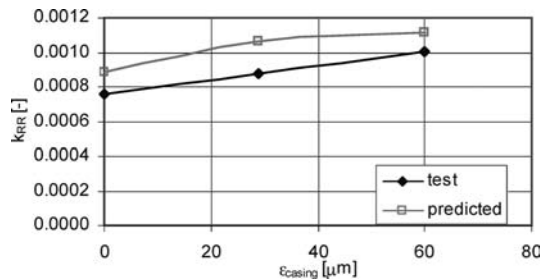


Fig. 3. Effect of casing roughness on disk friction (impeller side disks are smooth); test data from [18]

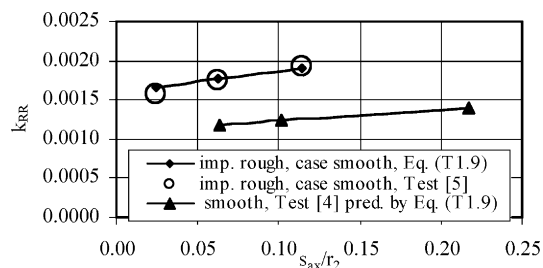


Fig. 4. Influence of axial casing width on disk friction factors; test data from [4 and 5]

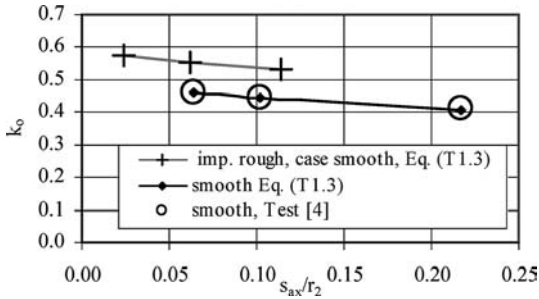


Fig. 5. Influence of axial casing width on rotation factor; test data from [4]

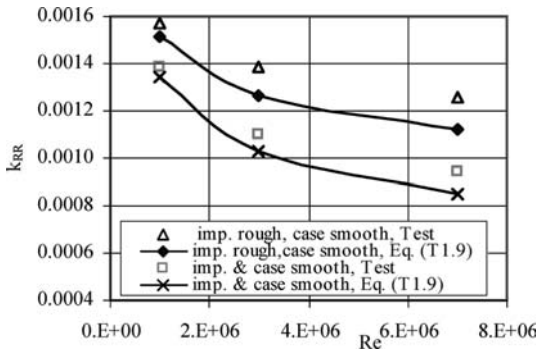


Fig. 6. Disk friction: rough impeller in smooth casing; test data from [17]

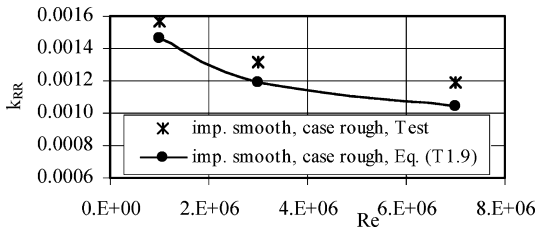


Fig. 7. Disk friction: smooth impeller in rough casing; test data from [17]

Eqs. (T1.3 and 1.9) as demonstrated by Figs. 3–7. Figure 3 shows disk friction factors derived from tests by Münch [18], where the pump efficiency was measured with smooth impeller side disks while the casing roughness in the side rooms was increased. While the trend with increasing casing roughness is well predicted by Eqs. (T1.3 and 1.9) the absolute values calculated are higher than those derived from the tests. One reason for this may be that some geometric dimensions (not given in [18]) had to be assumed for this comparison.

Figure 4 shows disk friction factors measured by Neece and Dailey [5] for a rough disk rotating in a smooth casing for various axial casing widths. The predictions by the formulae in Table 1 virtually coincide with the tests. Friction factors for a smooth disk are given for comparison. Figure 5 shows the rotation factors for the same data as in Fig. 4; prediction again agrees very well with testing, confirming thus Eq. (T1.3).

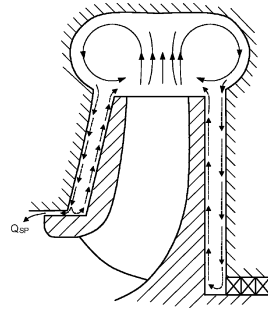


Fig. 8. Secondary flow influencing side room inlet whirl velocity when impeller discharges into volute

Geis [17] measured a rough impeller in a smooth casing (Fig. 6) and a smooth impeller in a rough casing (Fig. 7); again the prediction is quite good (the test data are slightly above prediction, because there was a small flow through the side room which slowed down the rotation (see discussion below).

3.3

Friction on cylindrical surfaces

The power loss created by any cylindrical parts of the impeller (hub, labyrinths, outer diameter of the shrouds) can be calculated from Eqs. (T1.13 and 14), [12, 14]. These formulae can also be used for cylindrical portions of axial thrust balancing devices.

4

Disk friction in turbomachines

Recognising that side room geometry and flow conditions in pumps can be quite different from a disk rotating in a cylindrical casing attempts have been made to measure disk friction in pump geometries with or without net flow through the side room.

4.1

Disk rotating in a volute casing

Some authors measured the power absorbed by disks rotating in a volute pump casing [20–22]; they found that the disk friction coefficients derived from such tests were typically 40 to 70% higher than those given in Fig. 2 and measured with disks rotating in cylindrical casings with r_w/r_2 little larger than 1.0. The reason for this apparent increase in disk friction can be seen from Eq. (T1.3): in tests with volute casings r_w/r_2 may be about 1.3–1.4 resulting in low rotation factors which, together with Eq. (T1.9), give indeed friction coefficients as high as measured with volutes. Measuring disk friction in volute casings leads to reduced k_o and increased k_{RR} because the whirl velocity c_u imparted on the fluid by the rotating disk is slowed down by friction on the large volute surface and dissipated by mixing losses created by velocity gradients and secondary flow, see Fig. 8. Nemdili [22] tested the disks also with a cylindrical cover which reduced the interaction of the flow in the side room with the volute flow. De-coupling volute and side room flow in this way gave smaller disk friction coefficients.

When a pump impeller rotates in a volute casing, flow conditions are entirely different from those in the above

Table 2. Rotation of the fluid in the impeller side room

		Eq.
Definitions	$\varphi_{sp} = \frac{Q_{sp}}{\pi r_2^2 u_2} \quad x = \frac{r}{r_2} \quad k = \frac{c_u}{u} = \frac{c_u}{\omega r} = \frac{\beta}{\omega}$	2.1
Side room inlet : development of rotation factor in overlap x_{ov} (Fig. 1); $z^* = z/r_2$ is the coordinate in axial direction. Stepwise calculation from $z^* = 0$ to $z_{max}^* = x_{ov}/r_2$	$\frac{dk}{dz^*} = \frac{c_{f,imp}(1-k)^2 - r_w^{*2} c_{f,case} F_{Form} k^2}{\frac{\varphi_{sp}}{2} + \frac{(r_w^* - 1)\varepsilon_z}{\omega r_2^2}}$ <p>F_{Form} is a form factor (usually 1.0). For $x_{ov} = 0$ no change in rotation is expected</p>	2.2
Friction factors (flat plate data)	$c_f = \frac{0.136}{\left\{ -\log\left(0.2 \frac{\varepsilon}{r_2} + \frac{12.5}{Re}\right) \right\}^{2.15}}$	2.3
Step-wise calculation of rotation, pressure coefficient and axial thrust coefficient	$\frac{dk}{dx} = \frac{0.079x^{1.6}}{\varphi_{sp} Re_u^{0.2}} \left\{ \left(\frac{1-k_0}{k_0} \cdot k \right)^{1.75} - 1-k ^{1.75} \right\} - 2 \frac{k}{x}$	2.4
	$k_{n+1} = k_n + \frac{dk}{dx} (x_{n+1} - x_n)$	2.5
Torque due to friction on an annular element of the disk	$dM^* \equiv \frac{dM}{\rho \omega^2 r_2^5} = \frac{0.287x^{3.6} 1-k ^{1.75} dx c_{f, Rough}}{Re_u^{0.2} c_{f, smoth}} \text{sign}(1-k)$	2.6
Disk friction coefficient from summation of all elements	$k_{RR} = \frac{\sum_n dM^*}{1 - d_{sp}^* 4.6}$	2.7
Calculation of average rotation factor from the integration of the pressure in the impeller side room	$k_{cp} = \sqrt{\frac{2(p_2 - p)}{\rho u_2^2 \left(1 - \frac{r^2}{r_2^2}\right)}}$	2.8
Estimation of leakage flow for normal clearances	$\varphi_{sp} = 5.5 \times 10^{-4} \psi_{opt}^{1.5} \left\{ \frac{n_q}{n_{q, Ref}} \right\}^{0.4} \quad n_{q, Ref} = 20$	2.9
Development of circumferential velocity component in a seal as function of the axial coordinate z . At seal inlet: $k_{in} = c_{u, in}/u_{sp}$ [19] Re_{ax} is with the axial Re_u the circumferential velocity of the seal	$k \equiv \frac{c_u}{u_{sp}} = 0.5 + (k_{in} - 0.5) \exp \left\{ -\frac{\lambda z}{4s} \left(1 + \frac{0.75}{1 + 4 \left[\frac{Re_{ax}}{Re_u} \right]^2} \right) \right\}$	2.10

Only for $\|\varphi_{sp} Re_u^{0.2}\| > 0.002$. 1. Leakage radially inwards: φ_{sp} is positive. Calculation of k from outer to inner diameter.
2. Leakage radially outwards: φ_{sp} is negative. Calculation of k from inner to outer radius

tests: the main flow issuing from the impeller channels has a strong circumferential velocity and any flow into the side room has a moment of momentum as given by Eq. (2) which tends to accelerate the side room flow and thus reduces disk friction (if $k_E > k_o$). Hergt and Prager [10] measured disk friction losses under real pumping conditions by using a test rig with a split rear shroud that way that rear shroud and impeller were driven by two different motors running at exactly the same speed. The disk friction power absorbed by the rear shroud could thus be measured separately from the impeller power, while the inlet flow conditions to the side room were given by the impeller outlet velocity. So far this approach appears to be the only way to correctly measure disk friction power under real pumping conditions.

4.2

Effect of net flow through side room

Kurokawa [23] solved the differential equations for side rooms with net through flow numerically and presented the results in a series of graphs in which the effects of leakage flow rate and pre-swirl at the side room inlet were lumped into one parameter. Zilling [7] and Möhring [8] developed a step-wise integration of the side room flow based on a force balance of moment of momentum per Eq. (2) and of drag forces on rotating and stationary surfaces. Lauer [11] derived a similar formula as [7] but included a second order term accounting for the effect of the turbulent shear stress ε_r . This yields a differential equation which must be solved numerically. The present investigation is based on the work of Möhring, but

some adaptations have been necessary in order to get a generic and numerically stable procedure. In particular for the side room inlet a new approach has been chosen. The side room calculation with net through flow is given in Table 2; it comprises the following steps:

1. The leakage flow rate Q_{sp} is assumed to enter the side room with the average circumferential velocity $c_{2u} = gH/(u_2\eta_h)$ at the impeller outlet. Hence φ_{sp} per Eq. (T2.1) and $k_E = c_{2u}/u_2$ are the boundary conditions for the calculation. If the leakage flows radially inwards, φ_{sp} is positive and the calculation of k proceeds from outer to inner diameter. If the leakage flows radially outwards, φ_{sp} is negative and the calculation of k proceeds from inner to outer radius.
2. If there is an overlap between impeller side disks and stator parts (see Fig. 1) the rotation of the fluid may be changed in this overlap due to drag on stator and rotating disk and due to turbulent shear stresses if the velocity of the main flow at the impeller outlet differs strongly from the side room rotational velocity. Equation (T2.2) allows to estimate the development of the rotation factor as a function of the axial coordinate z . Equation (T2.2) exhibits the following features, which correspond to the physical tendencies expected: (1) For $k = 0.5$ there is little change; $k = 0.5$ corresponds to the solution for the flow through a long axial gap. (2) If the roughness of the casing is higher than on the disk, the rotation tends to slow down. The same is true if the casing diameter is much larger than the impeller diameter (effect of r_w^*); all friction factors are calculated from Eq. (T2.3). (3) The higher the flow through the gap (φ_{sp}) the smaller the change in rotation, since drag forces are then less able to accelerate or decelerate a large mass flow. (4) With increasing turbulent shear stress (turbulent viscosity ε_τ) the effects of drag on the fluid rotation diminish because of the strong interaction of gap flow with main flow. (5) Equation (T2.2) works also for $\varphi_{sp} = 0$. The ratio of the turbulent to the molecular viscosity ε_τ/ν increases with the Reynolds-number and turbulence level. From Schlichting [15] maximum local values in pipe flow are about $\varepsilon_\tau/\nu = 0.016 \text{ Re}^{0.875}$ or $\varepsilon_\tau = 0.0028 \text{ m}^2/\text{s}$ for $\text{Re} = 10^6$ and $\nu = 10^{-6} \text{ m}^2/\text{s}$. Lauer [11] assumed $\varepsilon_\tau = 0.01 \text{ m}^2/\text{s}$ (3.6-times higher than in pipe flow). In view of the vortex shedding from the impeller blade trailing edges, strong velocity gradients at the impeller outlet and vortices created by shear flow between recirculating and forward flow during partload ε_τ may even exceed $0.01 \text{ m}^2/\text{s}$.
3. The change in rotation caused by the overlap (if any) is calculated by means of Eq. (T2.2) in a few steps Δz . The inlet condition k_z for the radial side room is thus defined at the exit of the overlap.
4. The rotation factor k_o is calculated from Eq. (T1.3). This equation does include the friction on the cylindrical stator part t_{ax} and on the surface element $\pi/4(r_w^2 - r_2^2)$ (see figure. in Table 1). This surface must therefore not be included in the overlap or side room inlet calculation (as has been done by others).

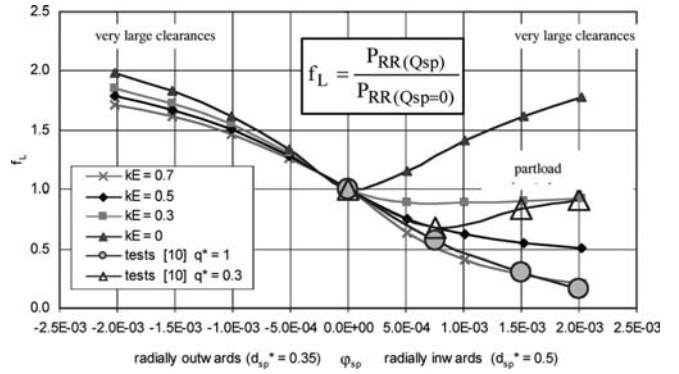


Fig. 9. Influence of leakage flow rate, direction and pre-rotation on disk friction

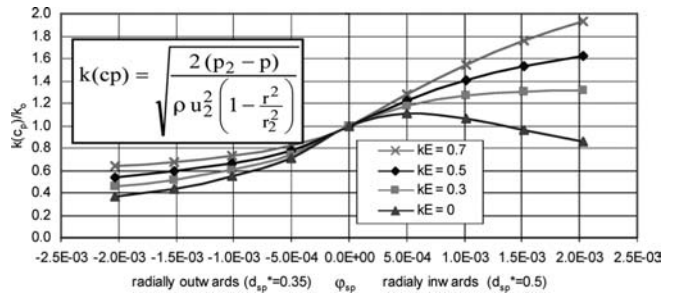


Fig. 10. Influence of leakage flow rate, direction and pre-rotation on rotation factor

5. The side room is calculated in radial steps of Δx starting at the impeller outer radius when leakage flows radially inwards. Equation (T2.4) gives the change in rotation in each step, while Eq. (T2.6) yields the torque on that radial element.
6. If the leakage flows radially outwards (inter-stage seal per Fig. 1), the calculation starts at inner radius $r_i = r_{s3}$ and progresses to the impeller outlet. The inlet conditions at r_i to the side room may be calculated from Eq. (T2.10) from Childs [19], which gives the circumferential velocity in an annular seal as a function of the axial coordinate.
7. The disk friction coefficient k_{RR} is the sum of all elements per Eq. (T2.7).
8. As the leakage flow is reduced the rotation factor k approaches k_o , dk/dx approaches zero and Eq. (T2.4) becomes $0/0$. If $k_E > k_o$ is imposed as boundary condition, Eq. (T2.4) yields then very high gradients dk/dx and the solution becomes numerically unstable. Equation (T2.4) should therefore be used for $|\varphi_{sp} \text{ Re}_u^{0.2}| > 0.002$ only; below this limit $k = k_o$ is a reasonable assumption.
9. The resulting distribution $k(r)$ can be integrated to get the pressure distribution and the axial thrust; details are given in [12]. Analytically integrating Eq. (T2.6) with $k = k_o$ yields Eq. (T1.9).

4.3

Influence of boundary conditions on disk friction

The formulae of Table 2 have been used to calculate the impact of leakage flow rate and direction on the disk friction coefficient and on the rotation factor. This has

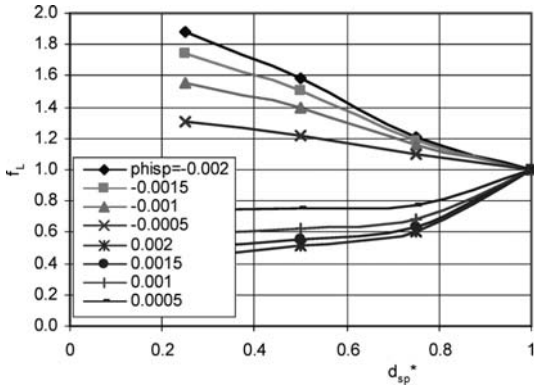


Fig. 11. Influence of inner diameter on disk friction; calculated with $k_E = 0.5$

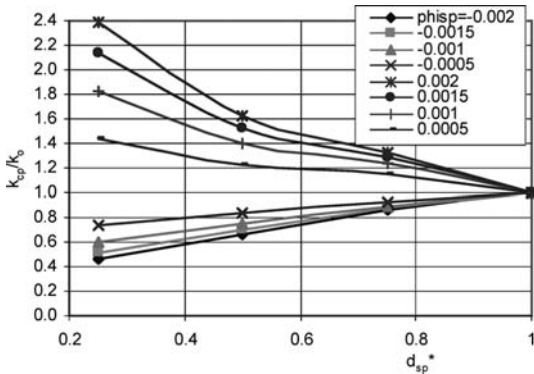


Fig. 12. Influence of inner diameter on rotation factor; calculated with $k_E = 0.5$

been done for various inlet conditions i.e. values of pre-rotation as defined by k_E . The following parameters have been selected: $Re = 1.3 \times 10^7$; $k_o = 0.45$; $x_{ov} = 0$ and sand roughness $\epsilon/r_2 = 2 \times 10^{-5}$. The results are shown on Figs. 9–12: the factor f_L accounts for the effect of leakage flow on disk friction and is defined by $f_L \equiv k_{RR}(Q_{sp})/k_{RR}(Q_{sp} = 0)$, while the ratio $k_{cp}/k_o = k(Q_{sp})/k_o(Q_{sp} = 0)$ describes the impact of leakage and pre-swirl on the rotation factor. The rotation factors plotted are average values calculated from the pressure profile on the impeller side disk according to Eq. (T2.8). Figures 9 and 10 show:

- Radially *inward* leakage: when $k_E > k_o$ fluid rotation grows, while disk friction decreases, with increasing leakage. For very large clearances disk friction can drop to a fraction only of the value with zero leakage flow. The tests by Hergt and Prager [10], done up to high net through flow, are well predicted by the formulae in Table 2.
- On the other hand disk friction losses *increase* with growing leakage when there is no pre-rotation ($k_E = 0$) or if pre-swirl is small ($k_E < k_o$). This can be the case during partload recirculation or if the impeller exit velocity distribution is strongly non-uniform.
- Surek [20], Möhring [8] and Geis [17] carried out their tests on rotating bodies with a leakage flow through the side room. With growing leakage flow rate disk friction

increased by a few per cent in these tests. This finding agrees with Fig. 9 for low values of k_E . The observed behaviour is however in contrast to operating turbo-machines, where inlet rotation k_E is high (except when operation at extremely high flow rates where head is close to zero). The reason for this appearing discrepancy is that the rotation imparted on the fluid at the side room entrance was too small in the tests quoted (k_E was appreciably smaller than k_o), even though it was attempted to impart a circumferential velocity component on the leakage flow prior its entering the side room. Münch [18] had the same problem in spite of considerable efforts to generate the same pre-rotation k_E as in the test pump.

- Radially *outward* leakage: with increasing leakage fluid rotation decreases and disk friction grows irrespective of pre-swirl k_E . But the effect of the leakage flow rate is mitigated by a strong pre-rotation. For very large clearances disk friction appreciably exceeds the value without net through flow. The impeller side disk then absorbs power in a way similar to a friction pump.

With increasing ratio of the inner to the outer radius (r_{sp}^* or r_{s3}^*) the impact of leakage flow on disk friction, fluid rotation and axial thrust decreases; it vanishes as this ratio approaches unity, Figs. 11 and 12.

Disk friction and rotation can not be presented by analytical expressions or simple correlations which take into account all of the parameters listed in (3). Equations (T1.11) and (T1.12) can however give an estimate for pump applications with $k_E \approx 0.5$. While Figs. 9–12 were calculated for the specific conditions defined above, these figures may be used as a first approximation to estimate the influence of Q_{sp} , k_E and d_{sp}^* .

It is obvious from the large variation of the fluid rotation, that leakage flow rate, direction and pre-swirl can have an important impact on axial thrust. Without correctly defining k_E and Q_{sp} axial thrust calculations can be grossly in error.

5 Conclusions

The procedures presented in Tables 1 and 2 allow the calculation of disk friction, fluid rotation and axial thrust taking into account the effects of roughness, leakage and pre-rotation at the side room inlet. The procedure agrees reasonably well with the test data presented in the literature quoted. Comparison of calculated and measured axial thrust confirms the validity of these procedures. When pumping highly viscous liquids the power absorbed by the pump increases compared to service in water. This is essentially due to disk friction only. Equations (T1.8) and (T1.9) predict this power increase well as demonstrated by [24] and [16].

The types of impellers covered by the method are:

- single-stage pumps without balancing holes: leakage on front shroud radially inwards; no leakage on rear shroud
- single-stage pumps with balancing holes: leakage on front and rear shroud radially inwards

- double-entry impellers: leakage on front and rear shroud radially inwards
- multi-stage pumps: leakage on front inwards on rear shroud outwards

As demonstrated by Figs. 9–12 the pre-swirl at the side room inlet has a very strong impact on fluid rotation and disk friction losses if leakage is high. The main uncertainties in predicting disk friction losses are: (1) the definition of the roughness (as discussed in detail in [16]) and (2) the determination of the inlet swirl. The actual circumferential velocity of the leakage flow entering the side room depends on the local velocity distribution at the impeller outlet, secondary flow patterns in volutes (Fig. 8) and on partload recirculation. Furthermore there is a close interaction between main flow, disk friction, leakage and fluid rotation. An undefined part of the disk friction power also adds useful energy to the main flow exiting the impeller (essentially that boundary layer flow thrown off the shrouds which has $c_u \geq c_{2u}$).

While pumps and compressors have similar flow conditions at the impeller outlet, for turbines the rotation k_E at the side room inlet must be defined from the flow distribution at the guide wheel (or volute) outlet.

References

1. Hamkins CP (2000) The surface flow angle in rotating flow: Application to the centrifugal impeller side gap. Diss. TU Kaiserslautern, Shaker Verlag, Aachen
2. Lingelbach T, Wiederuh E (1989) Die Axialschubberechnung radialer Turbomaschinen. Fortschrittber VDI Reihe 7, 154
3. Pantell K (1949/50) Versuche über Scheibenreibung. Forsch Ingenieurwes 16, 97–108
4. Dailey JW, Nece RE (1960) Chamber dimension effects on frictional resistance of enclosed rotating disks. ASME J. Basic Eng. 82, 217–232
5. Nece RE, Daily JW (1960) Roughness effects on frictional resistance of enclosed rotating disks. ASME J. Basic Engineering 82, 553–562
6. Fukuda H (1964) The effect of surface roughness on the performance of a Francis turbine. Bull. JSME 7(26), 346–356
7. Zilling H (1973) Untersuchung des Axialschubes und der Strömungsvorgänge im Radseitenraum einer einstufigen Radialpumpe. Strömungsmech Strömungsmasch H 15
8. Möhring UK (1976) Untersuchung des radialen Druckverlaufes und des Drehmomentes im Radseitenraum von Kreiselpumpen bei glatter, ebener Radseitenwand und bei Anwendung von Rückenschaufeln. Diss. TU Braunschweig
9. Schubert F (1988) Untersuchungen der Druck- und Geschwindigkeitsverteilung in Radseitenräumen radialer Strömungsmaschinen. Diss. TU Braunschweig
10. Hergt P, Prager S (1991) Influence of different parameters on the disc friction losses of a centrifugal pump. Conf on Hydraulic Machinery, Budapest, pp. 172–179
11. Lauer J (1999) Einfluß der Eintrittsbedingung und der Geometrie auf die Strömung in Radseitenräumen von Kreiselpumpen. Diss. TU Darmstadt
12. Gülich JF (1999) Kreiselpumpen. Ein Handbuch für Entwicklung, Anlagenplanung und Betrieb. Springer Berlin
13. Gülich JF et al. (1987) Review of parameters influencing hydraulic forces on centrifugal impellers. Proc. IMechE 201 (1987) A3, 163–174
14. Linneken H (1957) Der Radreibungsverlust, insbesondere bei Turbomaschinen. AEG Mitt 47(1/2), 49–55
15. Schlichting H (1982) Grenzschicht-Theorie. 8. Aufl, Braun, Karlsruhe
16. Gülich JF (2003) Effect of Reynolds-number and surface roughness on the efficiency of centrifugal pumps. Submitted to ASME J. Fluids Eng.
17. Geis H (1985) Experimentelle Untersuchungen der Radseitenverluste von Hochdruck-Wasserturbinen radialer Bauart. Diss. TH Darmstadt
18. Münch A (1999) Untersuchungen zum Wirkungsgradpotential von Kreiselpumpen. Diss. TU Darmstadt
19. Childs DW (1982) Dynamic analysis of turbulent annular seals based on Hirs' lubrication equation. ASME 82-Lub-41
20. Surek D (1966) Untersuchung der Radreibungs- und Undichtheitsverluste in Radialpumpen. Maschinenbautechnik 15(7), 353–358 and 15(8), 425–422
21. Osterwalder J, Ettig C (1977) Determination of individual losses and scale effect by model tests with a radial pump. Instnt. Mech. Engrs. Conf. Stirling, paper C 185/77, 105–111
22. Nemdili A (2000) Einzelverluste von Kreiselpumpen mit spezifischen Drehzahlen von $n_q = 15\text{--}35$ rpm. SAM Forschungsberichte, Bd 1, Diss. Uni Kaiserslautern
23. Kurokawa J, Toyokura T (1976) Axial thrust, disk friction torque and leakage loss of radial flow turbomachinery. Intl. Conf. on pump and turbine design NEL, Glasgow, Paper 5-2
24. Gülich JF (1999) Pumping highly viscous fluids with centrifugal pumps. World Pumps, Aug/Sept
25. Hergt P (1997) Hydraulic design of rotodynamic pumps. In: Hydraulic Design of Hydraulic Machinery. Rada Krishna (Hrsg), Avebury, Aldershot